Journal of Solid State Chemistry 183 (2010) 1632–1639

Contents lists available at ScienceDirect

Journal of Solid State Chemistry

journal homepage: www.elsevier.com/locate/jssc

From 2-D CuO nanosheets to 3-D hollow nanospheres: interface-assisted synthesis, surface photovoltage properties and photocatalytic activity

Jun Zhu, Xuefeng Qian*

School of Chemistry and Chemical Technology, State Key Laboratory of Metal Matrix Composites, Shanghai Jiao Tong University, Shanghai 200240, P R China

ARTICLE INFO

Article history:
Received 2 March 2010
Received in revised form
12 May 2010
Accepted 13 May 2010
Available online 19 May 2010

Keywords:
Cupric oxide
Hollow nanosphere
Interface-assisted synthesis
Bubble template
Surface photovoltage properties
Photocatalytic activity

ABSTRACT

CuO hierarchical hollow nanostructures, assembled by nanosheets, were successfully prepared in n-octanol/aqueous liquid system through a microwave approach. Controlled experiments revealed that both bubble and interface play key roles in determining the self-assembly process of CuO hierarchical hollow nanostructures, and the morphology/size of building blocks and final products could be readily tuned by adjusting reaction parameters. Furthermore, a self-assembly mechanism of aggregation-then-growth process through bubble template was proposed for the formation of the hollow hierarchical architectures. Photocatalytic performance evidenced that the obtained CuO hierarchical hollow nanostructures possessed superior photocatalytic efficiency on RhB than that of non-hollow nanostructures, which could be easily demonstrated by SPS response about the separation and recombination situation of photogenerated charges.

1. Introduction

The design and assembly of nanostructured building blocks into larger configurations in nanometer-to-micrometer dimensions have been developed rapidly in recent years. As a class of special organizations, hierarchical configurations with hollow structure have received much attention because of their peculiar structures and surface properties. Recently, considerable effort has been focused on the synthesis and properties of hierarchical hollow metal oxide organizations because of their important applications in heterogeneous catalysis, solar cells, sensors, and optical-electric devices [1–4]. However, the obtained hierarchical hollow metal oxide organizations composed by low-dimensional building blocks, such as In_2O_3, NiO, MnO_2, CuO, ZnO, WO_3, Fe_3O_4, Co_3O_4, and so on [5–12], are usually in micrometer dimension because of space encumbrance and loose aggregation or organization. Therefore, the fabrication of hierarchical hollow metal oxide configurations with complex geometrical structure in nanometer dimension is still a challenge.

In general, hierarchical hollow structures were synthesized through template-assisted process, or by direct self-assembly of primary structures without any external templates [13]. Among them, the template-assisted strategy is one of the most common methods to fabricate hollow micro/nanospheres because of their rich compositions, for example hard templates (silica, polymer or carbon particles) [14–16], soft templates (vesicles, emulsions, micelles) [17–19], or even gas bubbles [20]. In addition, some free surfactant/template approaches were also developed to prepare hollow structures, such as the self-assembled double-shelled ferrihydrite hollow spheres [21], 3D hierarchical self-assembled α-MnO_2 microstructures [22], and so on. Recently, some surprising and interesting structures or morphologies are also obtained through the synergic effect of different methods. For example, various hierarchical silica materials have been prepared by a dual-template method, such as zeolite, mesoporous silica, multilayered silica vesicles, hollow silica spheres with mesoporous shells, and so on [23–26]. Therefore, to pursue the research on more abundant morphology and dimension of hierarchical hollow configurations, cupric oxide (CuO) is served as a good model candidate because of its simple crystal structure and rich known morphologies.

As a p-type semiconductor, CuO exhibits a narrow band gap (1.2 eV). And it owns wide applications in the field of emission material, catalyst, gas-sensor, magnetic storage media, electronic, solar cell, and so on, because of its outstanding photoconductive and photochemical properties. Recently, well-defined CuO architectures with abundant dimensionality and morphology have been obtained successfully, in which one-dimensional (1-D) nanostructures are prevalent due to its nature, crystal growth habits or oriented attachment along the given crystal face of CuO nanocrystal. For example, nanoneedle, nanowire, nanowhisker, nanoshuttle, nanoleave, nanorod, nanotube and nanoribbon have been prepared by a

* Corresponding author. Fax: +86 21 54741297.
E-mail address: xfqian@sjtu.edu.cn (X. Qian).

0022-4596/$ - see front matter Crown Copyright © 2010 Published by Elsevier Inc. All rights reserved.
doi:10.1016/j.jssc.2010.05.015

series of chemical routes [27–34]. Furthermore, the advanced 2-D or 3-D CuO architectures, self-assembled by prime building blocks, are also reported. For example, Gao et al. [35] fabricated CuO hollow micro/nanostructures by a tyrosine-assisted hydrothermal system; Liu and Zeng [36] obtained macroscopic dandelions-shaped CuO microspheres, which were formed by rhombic building units from smaller nanoribbons via oriented aggregation. However, the reported hollow CuO architectures are usually in micrometer dimension and few of them are in nanoscale. In the present work, an NH_3 bubble-template and interface-assisted approach was designed to generate CuO hierarchical hollow structures with the size in nanoscale, the size and morphology of the obtained CuO nanostructure could be easily tuned by adjusting the size of NH_3 bubbles and the interface. Further results revealed that the obtained CuO hierarchical hollow nanostructures possessed superior photocatalytic efficiency on RhB than that of non-hollow nanostructures, and SPS response was used to demonstrate the separation and recombination situation of photogenerated charges.

2. Experiments

2.1. Preparation of materials

In the typical synthesis of sample A, 6 ml n-octanol was added into 5 ml $Cu(NH_3)_4^{2+}$ (0.05 M) clear aqueous solution, which was prepared by dissolving amount of $Cu(NO_3)_2 \cdot 3\,H_2O$ in ammonia (0.5 M). After being stirred and then maintained in still for another 2 h at room temperature in sealed Teflon vessel, obvious interface of n-octanol/aqueous solution was formed. Then the mixing solution was closed and placed in a conventional microwave oven with the power set to 100% of 1000 W and operated for 60 s (on for 20 s, off for 40 s) for reaction of 3 min. After the mixture was cooled to room temperature and kept to stand for at least 5 h naturally, white precipitate was suspended on the interface. And then final products were collected after being filtrated and washed with deionized water and ethanol several times, and dried in oven at 60 °C for 6 h.

Other samples were prepared in similar condition except for the concentration of $Cu(NH_3)_4^{2+}$, heating manner, alkaline source, interface style or the addition of SDS was changed. Detailed reaction condition and results were listed in Table 1.

2.2. Characterization

The obtained products were characterized by powder X-ray power diffraction (XRD, Shimadzu XRD-6000 instrument with Cu$K\alpha$ radiation, $\lambda = 1.5206$ Å). TEM images were recorded on a TEM (JEM100-CX transmission electron microscope) and HRTEM images were taken with a FEI SIRION 200 transmission electron microscope. SEM images were taken on a JSM-7401 F field-emission scanning electron microscope (SEM). FT-IR spectra were recorded on a Nicolet 5DX FT-IR instrument. The UV–vis adsorption spectra were carried on a Perkin Elmer UV–vis spectrophotometer LAMBDA 20 by dispersing samples in ethanol.

2.3. Photocatalytic activity measurement

The photocatalytic activity of the as-synthesized samples was evaluated for degradation of Rhodamine B (RhB) in an aqueous solution. Over 50 mg of photocatalyst sample was dispersed into the aqueous solution of RhB (50 mL) with a starting concentration of 1×10^{-5} M. Prior to irradiation, the suspension was magnetically stirred in dark for 5 min to establish an adsorption/desorption equilibrium between photocatalyst and RhB. At certain irradiation time intervals, aliquots of about 4 mL were withdrawn from the suspension and then filtered. The measurement of RhB concentration in the filtrate was carried out using a UV–vis spectrophotometer. The intensity of the absorption bands integrated at 550 nm was used to monitor the reaction progress. The percentage of decolorization at time t was calculated based on the equation, decolorization% $= (1 - A_t/A_0)100\%$, where A_0 and A_t were the integration areas for the initial RhB solution and the solution at reaction time t, respectively.

Table 1
The detailed reaction condition and corresponding results.

Sample	System	Alkali source	Heat manner	Concentration of Cu^{2+}	Amount of SDS	Morphology
A	Interface system	$NH_3 \cdot H_2O$	Microwave	0.05 M	0	The hierarchical hollow nanospheres with 500 nm in size assembled by nanosheet
B	Interface system	$NH_3 \cdot H_2O$	Microwave	0.01 M	0	The oblate structures with 800 nm in size assembled by nanosheet
C	Interface system	$NH_3 \cdot H_2O$	Microwave	0.1 M	0	The compact microspheres with 3 μm in size assembled by nanosheet
D	Interface system	$NH_3 \cdot H_2O$	Microwave	0.2 M	0	The disaggregated microspheres
E	Interface system	$NH_3 \cdot H_2O$	Microwave	0.3 M	0	The fused microspheres
F	Interface system	$NH_3 \cdot H_2O$	Reflux	0.05 M	0	The quasi-1-D array assembled by nanosheet
G	Interface system	NaOH	Microwave	0.05 M	0	Microsheets
H	Aqueous solution	$NH_3 \cdot H_2O$	Microwave	0.05 M	0	The microstrips besides microspheres
I	n-octanol system	$NH_3 \cdot H_2O$	Microwave	0.05 M	0	The nanorods with 100 nm in length
J	Interface system	$NH_3 \cdot H_2O$	Microwave	0.05 M	0.5%[a]	The hierarchical hollow nanospheres with 1 μm in size
K	Interface system	$NH_3 \cdot H_2O$	Microwave	0.05 M	0.7%	The broken microsphere besides nanosheets
L	Interface system	$NH_3 \cdot H_2O$	Microwave	0.05 M	1.0%	The rice-like nanostructures with 300 nm in length and 100 nm in width

[a] The mass percent of SDS is the ratio of the mass of SDS to the total reaction system mass.

2.4. Surface photovoltage spectroscopy (SPS) measurement

Monochromatic light was obtained by passing light from a 500 W xenon lamp (CHF XQ500W, Global xenon lamp power made in China) through a double-prism monochromator (Hilger and Watts, D 300 made in England). The slit width of entrance and exit was 1 mm, and a lock-in amplifier (SR830-DSP, made in USA), synchronized with a light chopper (SR540, made in USA), was employed to amplify the photovoltage signal. The range of modulating frequency was from 20 to 70 Hz and the spectral resolution was 1 nm. The raw SPS data were normalized using the illuminometer (Zolix UOM-1S, made in China). During the SPS measurements, the contact between samples and indium tin oxide (ITO) electrode was not ohmic contact to measure the surface photovoltage. The photovoltaic cell was ensured that the light penetrating depth was much less than the thickness of powder layer. The potential of irradiated electrode with respect to the back electrode denoted the signs of the applied electrical field.

3. Results and discussion

3.1. Structure and morphology of CuO hierarchical hollow nanospheres

Because of the poor solubility of n-octanol in water and vice versa, the interface of n-octanol/water system can be easily formed. After the n-octanol/water system containing $[Cu(NH_3)_4]^{2+}$ was treated by microwave heating approach, NH_3 was produced quickly and the system was supersaturated by NH_3 bubbles, meanwhile CuO nucleus was formed. Thus CuO hierarchical hollow nanospheres were obtained on a large scale. The whole process can be expressed as following:

$$[Cu(NH_3)_4]^{2+} + 2H_2O \rightarrow Cu(OH)_2 + 2NH_4^+ + 2NH_3\uparrow$$

$$Cu(OH)_2 \rightarrow CuO + H_2O$$

The crystal phase of the as-synthesized products was identified by powder X-ray diffraction (XRD). Fig. 1a shows the typical XRD pattern of the sample obtained from n-octanol/$[Cu(NH_3)_4]^{2+}$ aqueous solution system (Sample A), which reveals clearly that all diffraction peaks match well with the pure monoclinic phase of CuO (JCPDS card no. 05-0661) with lattice constants $a=4.68$ Å, $b=3.43$ Å and $c=5.13$ Å. No other peaks are observed, indicating the high purity and well crystallinity of the obtained sample. EDX spectrum also reveals that the atomic ratio of Cu:O is equal to 1:1 in the obtained sample (Fig. 1b). Other samples prepared in the present work are also in pure monoclinic CuO phase.

Typical CuO nanostructures were prepared in n-octanol/$[Cu(NH_3)_4]^{2+}$ aqueous solution system at 0.05 M $[Cu(NH_3)_4]^{2+}$ through microwave heating (sample A). Fig. 2 displays the general morphology of sample A. Uniform spherical CuO nanostructures with the average size of about 600 nm are the exclusive products in SEM image (Fig. 2a), indicating that CuO nanospheres can be prepared on

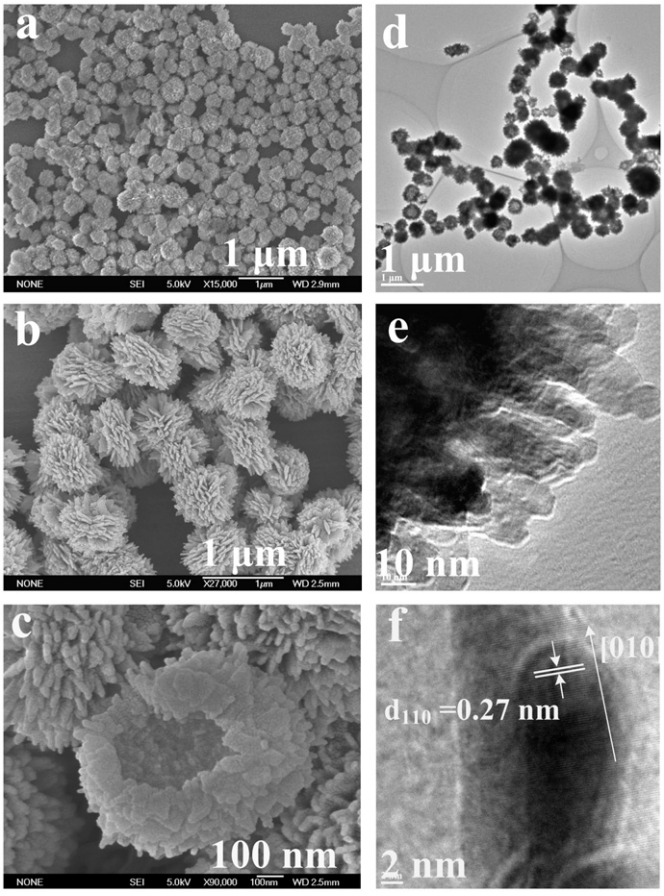

Fig. 2. SEM and TEM images of CuO obtained in n-octanol/$[Cu(NH_3)_4]^{2+}$ aqueous solution system at 0.05 M $[Cu(NH_3)_4]^{2+}$ through microwave heating. (a) Low-magnification SEM image, (b) enlarged SEM image, (c) FESEM image, (d) low-magnification TEM image, (e) enlarged TEM image and (f) HRTEM image.

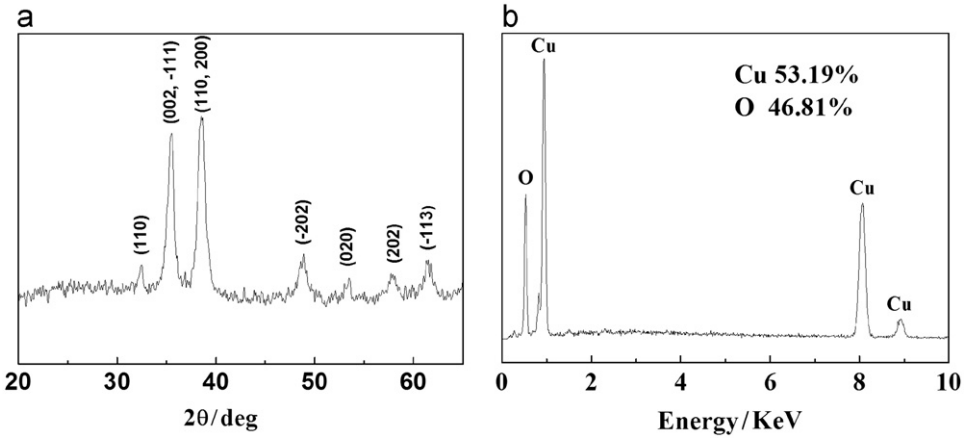

Fig. 1. Typical (a) XRD and (b) EDX patterns of sample obtained in n-octanol/$[Cu(NH_3)_4]^{2+}$ aqueous solution system at 0.05 M $[Cu(NH_3)_4]^{2+}$ through microwave heating process.

a large scale. Enlarged SEM image (Fig. 2b) shows that the obtained CuO nanospheres are in hierarchical structure with rough appearance and constructed by 2-D sheet-like CuO nanocrystals. Closer observation reveals that the assembled nanocrystals are on an ordinal layer-built manner, which is different from the usual interlaced network-like morphology in many reports. The FESEM image of an individual cracked 3-D CuO nanosphere further supports the observation (Fig. 2c). To our surprise, the 3-D CuO nanospheres are in hollow structure, the thickness of CuO nanosphere shell and the diameter of cavity are about 100 and 400 nm, respectively. Meanwhile, FESEM image also reveals that the obtained nanospheres are assembled closely by nanosheets with about 10 nm in thickness. TEM image (Fig. 2d) further indicates clearly that the obtained CuO sample is in spherical nanostructure, and the obvious difference in terms of contrast between the central and fringe part of individual particle also implies the hollow structure of the obtained products. The structure of the obtained CuO is similar to the report of Zeng [36] except for the smaller size. Enlarged TEM image (Fig. 2e) further reveals clearly that the subunits of CuO hierarchical hollow nanostructure are in nanosheet shape. The HRTEM image (Fig. 2f) taken from the head part of individual CuO nanosheet indicates the single crystalline nature of CuO nanosheet. The 0.27 nm spacing of crystallographic planes corresponds to the [1 1 0] lattice fringe of monoclinic CuO, indicating its growth along [0 1 0] direction. The formation of CuO nanosheet is similar to the previous reports because the growth of primary CuO nanocrystals in three directions is substantially different and follows the order: [0 1 0] > [1 0 0] ≫ [0 0 1] [27,29,30]. Additionally, the sharing identical lattices between adjacent nanosheets (Fig. 2f) also give direct evidences that the self-assembly of nanospheres undergoes the "Oriented Attachment" process.

3.2. Influence of the concentration of $Cu(NH_3)_4^{2+}$ on CuO architectures

In the present work, it is found that the concentration of $Cu(NH_3)_4^{2+}$ has important effect on the morphology of final products (samples B–E). When the concentration of $Cu(NH_3)_4^{2+}$ is 0.01 M, oblate-like CuO architectures assembled by nanosheets are obtained (Fig. 3a). However, compared to Fig. 2b, the assembled oblate-like CuO (about 800 nm in dimension) is in irregular shape and loose structure. Increasing $Cu(NH_3)_4^{2+}$ concentration to 0.1 M, the size of the obtained spherical CuO increases obviously (about 3 μm in dimension) (Fig. 3b). Meanwhile, the surface of the obtained microspheres becomes smoother, resulting from the compact aggregation of CuO nanosheets. If the concentration of $Cu(NH_3)_4^{2+}$ is further increased to 0.2 M, CuO microspheres have a tendency to fuse each other, and entangled networks are formed coexistent with spherical CuO structures (shown in Fig. 3c). With further increasing $Cu(NH_3)_4^{2+}$ concentration to 0.3 M, the amalgamation of CuO spheres becomes serious and entangled network-like CuO are dominant (Fig. 3d).

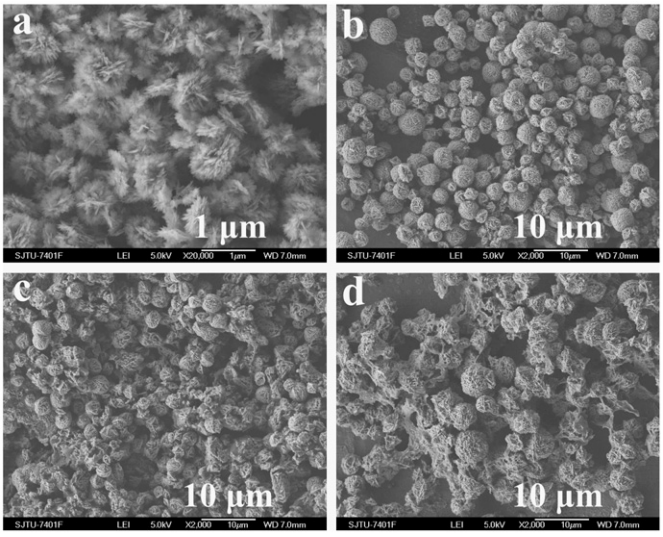

Fig. 3. SEM images of CuO obtained in n-octanol/$[Cu(NH_3)_4]^{2+}$ aqueous solution system with $NH_3 \cdot H_2O$ as alkali source through microwave heating with different concentrations of $Cu(NH_3)_4^{2+}$: (a) 0.01 M, (b) 0.1 M, (c) 0.2 M and (d) 0.3 M.

3.3. Influence of alkaline source and heating manner on CuO architectures

Recently, a bubble-template strategy was proved to be one of the most promising approaches to prepare hierarchical hollow spheres. For example, hierarchical hollow spheres of TiO_2 and ZnSe built by 0-D nanoparticles have been prepared through hydrothermal process [37]; hollow VOOH with the "dandelion" shape assembled by advanced 1-D or 2-D subunits has been obtained through the bubble-template strategy [38]. In addition, an interface-assisted method has been used to prepare a number of materials due to its simplicity, low cost and scalability, such as pyramidal PbS nanocrystals, CeO_2 nanocrystal assemblies, CdSe nanocrystal assemblies, ultrathin single-crystalline sheets of CuS and ordered arrays of Cu_2S nanocrystals [39–43]. Furthermore, the synergic synthesis and assembly on liquid–liquid interface would usually lead to the construction of functional materials. For example, the growth and assembly of TiO_2 nanorods into hierarchical spheres could be realized on soft interface between water and chloroform in one-step [44]. So it is reasonable to believe that the formation of 3-D hollow CuO architectures is attributed to NH_3 bubbles in the liquid–liquid interface system. To better understand the effects of NH_3 bubbles for the assembly of CuO nanosheet to hollow nanospheres, controlled experiments were performed in an open reflux system at 140 °C for 12 h (sample F), and the products, collected on the interface of n-octanol/aqueous solution, looked like a layer of film on the interface, which is popular architecture in interface-assisted synthesis [40]. As shown in Fig. 4a, the film is also assembled by irregular nanosheets, which are similar to the subunits of hollow CuO nanospheres in Fig. 2c except for the larger size (500 nm in length). Under our knowledge, the releasing rate of NH_3 depended on the reaction rate and reaction temperature. Compared to microwave reaction, the slower releasing rate of NH_3 would lead to NH_3 bubbles running out if the reaction was carried out in an open reflux system at 140 °C, which would further result from the dispersed nanosheets. Therefore, the growth and assembly of these nanosheets on the interface of n-octanol/aqueous solution lead to the quasi-array of nanosheets. In order to further understand the effect of NH_3 on the formation of hollow structure, ammonia was replaced by NaOH in the n-octanol/$Cu(NO_3)_2$ aqueous solution system (sample G), only CuO microsheets were obtained (Fig. 4c). These obtained CuO microsheets have uniform size and morphology of about 1.5 μm in length, 400 nm in width and 10 nm in thickness, respectively (Fig. 4d). The above results further demonstrate that NH_3 bubbles play a key role on the assembly of nanosheets and the formation of final hollow structure.

3.4. Influence of air/liquid interface system on CuO architectures

Furthermore, the interface system is also crucial for the formation of CuO hollow nanospheres. If only $[Cu(NH_3)_4]^{2+}$

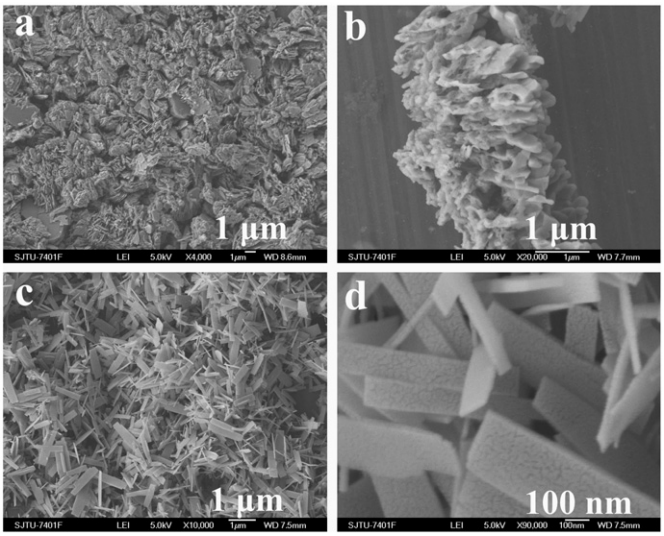

Fig. 4. SEM images of CuO obtained with different alkali source or heating manner. (a and b) in n-octanol/$[Cu(NH_3)_4]^{2+}$ aqueous solution system at 0.05 M $Cu(NH_3)_4^{2+}$ with $NH_3 \cdot H_2O$ as alkali source through reflux process; (c and d) n-octanol/$Cu(NO_3)_2$ aqueous solution system at 0.05 M Cu^{2+} with NaOH as alkali source through microwave heating process.

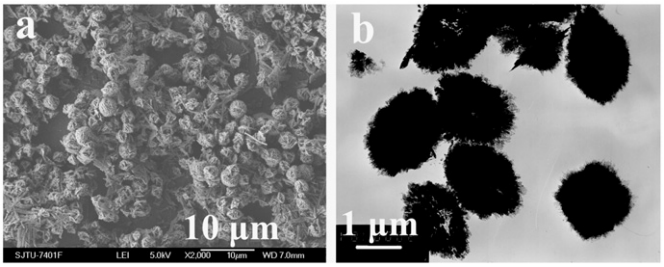

Fig. 5. (a) SEM and (b) TEM images of CuO obtained at 0.05 M Cu^{2+} in $[Cu(NH_3)_4]^{2+}$ aqueous solution system with $NH_3 \cdot H_2O$ as alkali source through microwave heating process.

aqueous solution, without n-octanol as interface, was microwave-heated in the similar condition (sample H), microspheres in loose sphere-like morphology are obtained besides some of the 1-D strip-like microstructures (Fig. 5a). TEM image (Fig. 5b) shows that the obtained solid microspheres are about 2 μm in diameter (much larger than that of nanospheres in Fig. 2b). In n-octanol/aqueous liquid interface system, the interface can stabilize and confine the released NH_3 bubbles in solution phases from escaping from the n-octanol phase because of the high viscoelasticity of n-octanol, which would serve as template for the formation of hollow CuO spheres. However, in air/aqueous liquid interface system, the quickly released NH_3 bubbles tend to escape from aqueous liquid, which is much different from the reported bubble or half-bubble templates yielded in mild conditions in a similar system [45,20,37]. Therefore, the produced CuO crystal in aqueous liquid tends to form microspheres through self-assembly driven by the minimum system energy [36], or tend to further grow into 1-D CuO because of its anisotropic crystal structure in nature under the unrestricted condition [27,29,30].

3.5. Formation mechanism of CuO hierarchical hollow nanospheres

Based on our experiments, an aggregation-then-growth process through NH_3 bubble template was proposed for the formation of CuO hierarchical hollow nanospheres. As illustrated in Fig. 6, when the mixed solution was heated by microwave irradiation, large amounts of NH_3 were erupted from $[Cu(NH_3)_4]^{2+}$ aqueous solution due to the hydrolyzation of $[Cu(NH_3)_4]^{2+}$, resulting in the water-rich phase supersaturated with NH_3 bubbles in few seconds, and then the NH_3 bubbles on the n-octanol/aqueous liquid interface acted as templates for the aggregation of CuO nuclei. On the other hand, the freshly formed crystalline primary nanostructures were unstable because of their high surface energy and they tended to aggregate around the gas/liquid interface of NH_3 bubbles so as to protect NH_3 bubble from enlarging, driven by the minimization of interfacial energy. Furthermore, the controlled experiments also indicated that the building blocks of CuO hierarchical hollow nanospheres were in 1-D structure and they aggregated around NH_3 bubble with the help of n-octanol, because 1-D CuO was formed if the experiment was performed in pure n-octanol system (sample I), which was similar to popular nanoparticle or nanorod through microwave synthesis process [46,47]. The FT-IR spectra of the obtained product also revealed the absorption of n-octanol molecule on the obtained 1-D CuO nanomaterials (Supporting Information 1). Thus, the continuous aggregation process of 1-D CuO occurred and hollow spheres were formed. Then the adjacent 1-D CuO further grew into nanosheets relating to the nature of initial crystal, and CuO hollow spheres assembled by nanosheets were formed finally. The formation process is similar to the reported VOOH hollow "dandelions" organized from flake building blocks, in which the aggregation-then-growth process with N_2 bubble as template was proposed [38].

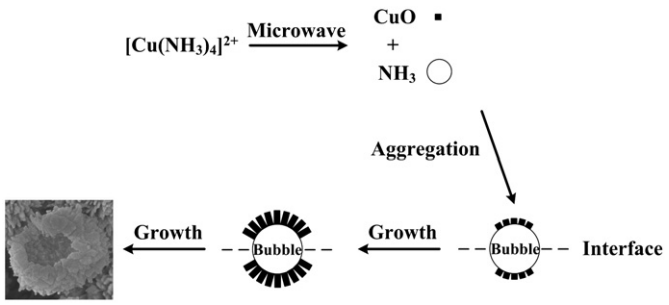

Fig. 6. Schematic illustration of the growth process of CuO hierarchical hollow architectures.

3.6. Influence of SDS on CuO architectures

In general, surfactant may affect the morphology of the obtained materials. In present system, sodium dodecyl sulfate (SDS) was chosen as model surfactant to study its effect on the size and shape of the obtained CuO. When 0.5% SDS was introduced into the reaction system (sample J), larger CuO spheres with the average size of about 1 μm are obtained in a large scale (Fig. 7a). Compared to Fig. 2b, the obtained CuO spheres have more slippery surface, and they are packed by nanosheets compactly. TEM image (Fig. 7b) also shows that the obtained CuO spheres are packed by higher density CuO nanosheets. Careful observation reveals that these CuO spheres are also in hollow structure though it is difficult to be observed in the TEM image because of the compact pack of CuO nanosheets. However, FESEM image of one broken sphere clearly reveals that the obtained CuO spheres are in hollow structure (Supporting Information 2), and this observation also confirms that CuO spheres are assembled by nanosheets. On the other hand, the surface area of the as-prepared CuO architectures decreases from 13 m^3/g (sample A) to 8 m^3/g (sample J) with increasing size of CuO nanospheres, depending on the synthetic conditions. According to

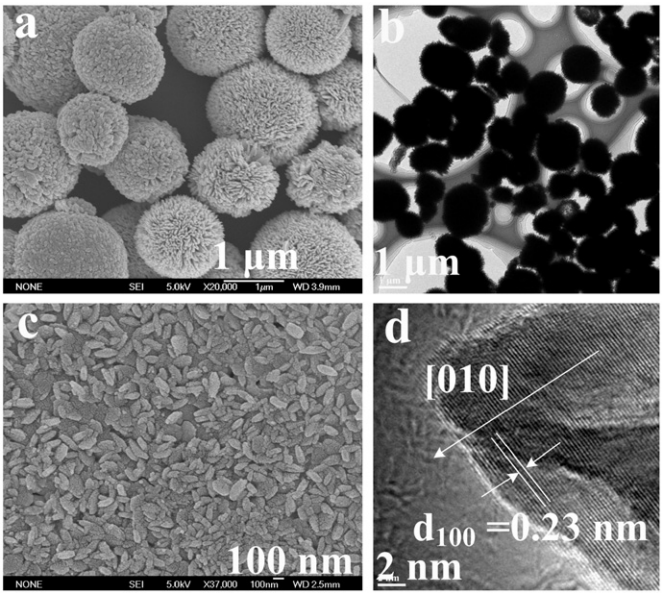

Fig. 7. (a) SEM and (b) TEM images of CuO obtained in n-octanol/0.5% SDS/$[Cu(NH_3)_4]^{2+}$ aqueous solution system at 0.05 M $[Cu(NH_3)_4]^{2+}$ with $NH_3 \cdot H_2O$ as alkali source through microwave heating process; (c) SEM and (d) HRTEM of CuO obtained in n-octanol/1.0% SDS/$[Cu(NH_3)_4]^{2+}$ aqueous solution system at 0.05 M Cu^{2+} with $NH_3 \cdot H_2O$ as alkali source through microwave heating process.

the calculated specific surface area ($S=6(\varnothing_1^2+\varnothing_2^2)/(\varnothing_1^3-\varnothing_2^3)\rho$) of hollow spheres with an outer diameter ($\varnothing_1$) and an inner diameter ($\varnothing_2$), the decrease of S and the increase of $\varnothing_1$ (compared to that of sample A) would result in the decrease of $\varnothing_2$ of sample B, which further confirm that the pores of sample J are smaller than those of sample A. However, both the surface areas of these samples are much smaller because of smaller dimension of the as-prepared samples. However, when the amount of SDS is increased to 1%, rice-like nanostructures, instead of nanospheres, are obtained (sample L, Fig. 7c), and rice-like nanostructures are about 300 nm in longitudinal axis and 100 nm in horizontal axis, respectively. HRTEM image (Fig. 7d) shows that nanosheets are still the basic building blocks for the rice-like structures. Meanwhile, the 0.23 nm lattice interplanar spacing is corresponding to the (2 0 0) plane of monoclinic CuO, which further indicates the [0 1 0] direction of the long-axis. To further evaluate the evolvement of CuO morphology from hollow sphere to rice-like nanostructure, 0.7% SDS was introduced to the reaction system (Supporting Information 3). The results show that CuO spheres are broken and some sheet-like CuO nanostructures are formed. The above results indicate that the addition of SDS goes against the aggregation CuO nanostructure and the shape of CuO nanostructure changes from sphere to nanosheets with the increase of SDS. As we know, the additional SDS molecules could not only increase the intension of NH_3 bubbles and the interface of n-octanol/$[Cd(NH_3)_4]^{2+}$ aqueous solution system, but also absorb on CuO nanocrystals to increase the hydrophobic interaction for further aggregation of CuO nanocrystals. However, as shown in Fig. S4, different contents of SDS have different effect on NH_3 bubbles, n-octanol/$[Cd(NH_3)_4]^{2+}$ interface or primary CuO crystal, which results in the change of final CuO morphologies (Supporting Information 4).

3.7. Photocatalytic performance of CuO architectures

In the present work, Rhodamine B (RhB) was chosen as a representative organic dyestuff to evaluate the photocatalytic performance of CuO architectures with different morphologies. Fig. 8a displays the typical time-dependent UV–vis absorption spectra of RhB solution during the photodegradation in the presence of hierarchical hollow nanospheres, in which RhB displays its maximum absorption peak at around 550 nm. During the course of degradation, the color of RhB solutions became less intense, and the intensity of absorption spectra decreased gradually with irradiation time increasing, implying a strong oxidation of RhB had occurred in the presence of hollow hierarchical nanospheres under UV–visible light. Fig. 8b shows the decolorization plots of RhB over irradiation time in the presence of CuO architecture with morphologies, such as hierarchical hollow nanospheres (Sample A) and microsheets (Sample G). Except for the self-degradation of RhB due to the thermal effect especially by light illumination (curve 1), the photocatalytic rate of RhB in presence of CuO is faster. Compared to the decolorization curves 2 and 3, about 40% and 65% of RhB decolorization was achieved at 100 min in the presence of microsheets and hierarchical hollow nanospheres, respectively. Hence, one can see that CuO hierarchical hollow nanospheres possess superior photocatalytic activity for RhB degradation relative to that of CuO microsheets.

As well known, the photocatalytic property is the result of the co-effects of material's morphology and size, specific surface area, charge-carrier dynamics and light absorption efficiency. The previous references reveal that the hierarchical hollow nanostructure and the decrease of particle size usually increase the photocatalytic activity of catalyst [48,49]. Thus, we prefer to believe that the superior photocatalytic activity for RhB degradation is relative to the hierarchically aggregation-based CuO nanosheets and the smaller size of these building blocks of hierarchical hollow nanosphere. Moreover, the separation situation of photoinduced charges is one of the most important factors influencing the photocatalytic activity of semiconductor photocatalysts [50]. On the other hand, photoinduced holes can be easily captured by chemisorbed surface hydroxyl groups to produce hydroxyl radicals ($\cdot OH$); while electrons can be trapped by adsorbed O_2 to produce superoxide radicals (O_2^-). And both the radicals are usually responsible for the oxidation process of organic substances. Recently, SPS method is proved to be one of the most effective methods to reflect the separation and recombination situation of photogenerated charges to a certain extent [51]. Fig. 9a shows the SPS response of hierarchical CuO hollow nanospheres and CuO microsheets, respectively. One can see that three surface photovoltaic (SPV) response bands at 365, 405 and 470 nm appear in the SPV response of CuO hierarchical hollow nanospheres. Among them, the SPV signal at 365 nm corresponds to the UV–vis absorption band at 362 nm (Fig. 9b), due to the electron transitions from valence to conduction band (band-to-band transitions); The SPS peaks at 405 and 470 nm, situated near the energy band edge, are ascribed to the surface states [52]. The strongest SPV response at 365 nm implies a small number of surface states in CuO hierarchical hollow nanospheres. However, the SPV response of CuO microsheets at 470 nm becomes strongest (the enlarged SPV response curve inserted in Fig. 9a), leading to the increasing surface states going against the band-to-band transitions, the separation situation of photoinduced charges and further its photocatalytic activity [49]. In addition, it is obvious that the SPS response of CuO hierarchical hollow nanospheres is much stronger than that of CuO microsheets, which implies that the photogenerated electrons and holes of CuO hierarchical hollow nanospheres can be effectively separated. As a result, the photocatalytic activity of CuO hierarchical hollow nanospheres is superior to that of CuO microsheets. Moreover, similar results can be found in UV–vis absorption spectra of CuO hierarchical hollow nanospheres and CuO microsheets (Fig. 9b). The absorption band of CuO microsheets

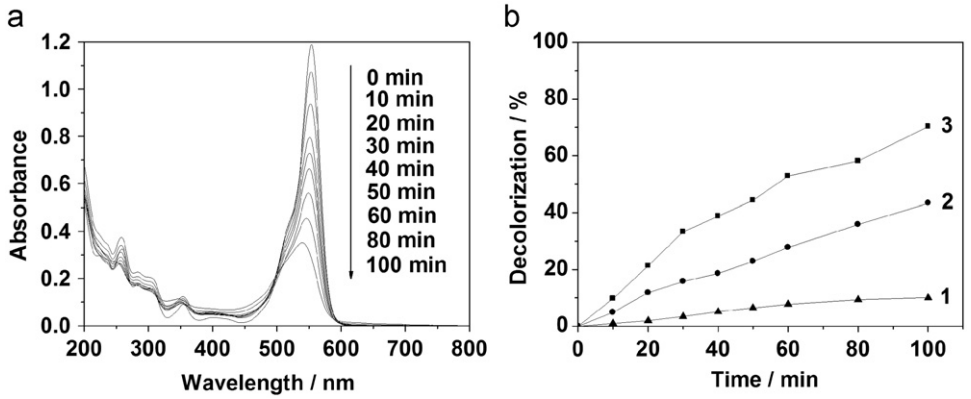

Fig. 8. (a) Typical time-dependent absorption spectra of RhB solution in the presence of hierarchical hollow nanospheres under UV–visible light irradiation, (b) photocatalytic degradation of RhB under different conditions: 1—in the absence of photocatalysts, 2—microsheets and 3—hierarchical hollow nanospheres.

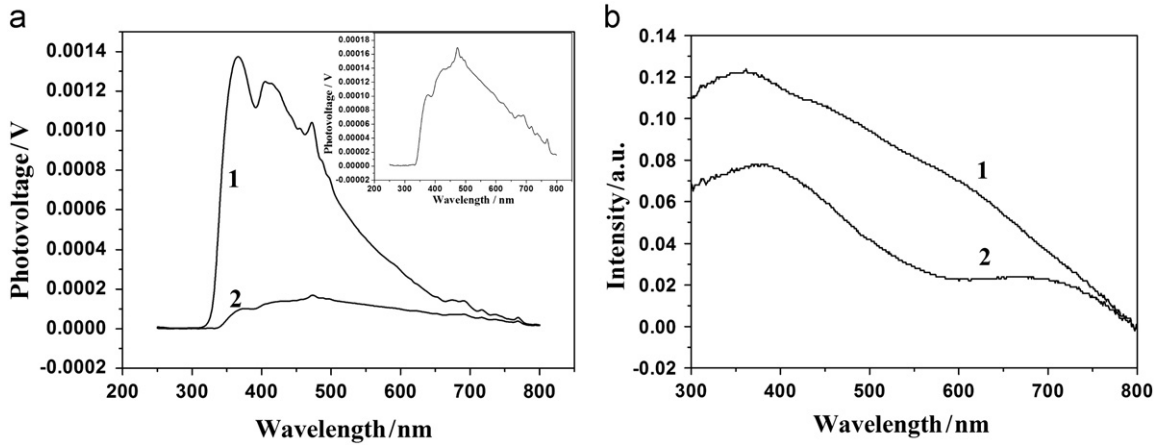

Fig. 9. (a) SPS response and (b) UV–vis absorption spectra of hierarchical CuO hollow nanospheres and CuO microsheets: 1 – CuO hierarchical hollow nanospheres and 2 – CuO microsheets.

is red shifted from 362 nm of CuO hierarchical hollow nanospheres to 382 nm, which also results in the narrower band gap of CuO. Furthermore, the result is not favorable for the separation of photoinduced charges, leading to its low photocatalytic activity.

4. Conclusion

CuO hierarchical hollow nanostructures with the size in nanometer, assembled by nanosheet building blocks, were successfully prepared through a novel double-soft-template approach, and a possible mechanism of aggregation-then-growth was proposed. Controlled experiments revealed that the morphologies of the building blocks and the final products could be easily adjusted by the reaction parameters, including precursors, heating manners, interface style and alkali source et al. The addition of surfactant SDS could adjust the size of NH_3 bubble so as to control the size and morphology of the obtained CuO nanostructure. Furthermore, it was found that the CuO hierarchical hollow nanostructure could improve its photocatalytic efficiency on RhB than that of non-hollow nanostructure. SPS response further demonstrated that the band-to-band SPS response of CuO hierarchical hollow nanospheres is beneficial for the separation situation of photoinduced charges, and further improved its photocatalytic activity.

Acknowledgments

The work described in this paper was supported by the National Science Foundation of China (no.: 20671061), National Basic Research Program of China (2009CB930400) and the Program for New Century Excellent Talents of Education Ministry of China.

Appendix A. Supporting information

Supplementary data associated with this article can be found in the online version at doi:10.1016/j.jssc.2010.05.015.

References

[1] Z.Q. Li, Y. Ding, Y.J. Xiong, Q. Yang, Y. Xie, Chem. Commun. 7 (2005) 918–920.
[2] A.D. Dinsmore, M.F. Hsu, M.G. Nikolaides, M. Marquez, A.R. Bausch, D.A. Weitz, Science 298 (2002) 1006–1009.
[3] Z.Y. Zhong, Y.D. Yin, B. Gates, Y.N. Xia, Adv. Mater. 12 (2000) 206–209.
[4] K.T. Lee, Y.S. Jung, S.M. Oh, J. Am. Chem. Soc. 125 (2003) 5652–5653.
[5] H.X. Dong, Z.H. Chen, L.X. Sun, L. Zhou, Y.J. Ling, C.Z. Yu, H.H. Tan, C. Jagadish, X.C. Shen, J. Phys. Chem. C 113 (2009) 10511–10516.
[6] Y. Wang, Q.S. Zhu, H.G. Zhang, Chem. Commun. 41 (2005) 5231–5233.
[7] M.W. Xu, L.B. Kong, W.J. Zhou, H.L. Li, J. Phys. Chem. C 111 (2007) 19141–19147.
[8] H.G. Zhang, Q.S. Zhu, Y. Zhang, Y. Wang, L. Zhao, B. Yu, Adv. Funct. Mater. 17 (2007) 2766–2771.

[9] X.F. Song, L. Gao, J. Phys. Chem. C 112 (2008) 15299–15305.
[10] D. Chen, J.H. Ye, Adv. Funct. Mater. 18 (2008) 1922–1928.
[11] S.W. Cao, Y.J. Zhu, M.Y. Ma, L. Li, L. Zhang, J. Phys. Chem. C 112 (2008) 1851–1856.
[12] A.M. Cao, J.S. Hu, H.P. Liang, L.J. Wan, Angew. Chem. Int. Ed. 44 (2005) 4391–4395.
[13] X.W. Lou, L.A. Archer, Z.C. Yang, Adv. Mater. 20 (2008) 3987–4019.
[14] V. Salgueirino-Maceira, M. Spasova, M. Farle, Adv. Funct. Mater. 15 (2005) 1036–1040.
[15] N. Kawahashi, C. Persson, E. Matijevic, J. Mater. Chem. 1 (1991) 577–582.
[16] Y.D. Xia, R. Mokaya, J. Mater. Chem. 15 (2005) 3126–3131.
[17] H.P. Hentze, S.R. Raghavan, C.A. Mckelvey, E.W. Kaler, Langmuir 19 (2003) 1069–1074.
[18] C.E. Fowler, D. Khushalani, S. Mann, Chem. Commun. 19 (2001) 2028–2029.
[19] J.X. Huang, Y. Xie, B. Li, Y. Liu, Y.T. Qian, S.Y. Zhang, Adv. Mater. 12 (2000) 808–811.
[20] X.X. Li, Y.J. Xiong, Z.Q. Li, Y. Xie, Inorg. Chem. 45 (2006) 3493–3495.
[21] Z.C. Wu, M. Zhang, K. Yu, S.D. Zhang, Y. Xie, Chem. Eur. J. 14 (2008) 5346–5352.
[22] P. Umek, A. Gloter, M. Pregelj, R. Dominko, M. Jagodič, Z. Jagličić, A. Zimina, M. Brzhezinskaya, A. Potočnik, C. Filipič, A. Levstik, D. Arčon, J. Phys. Chem. C 113 (2009) 14798–14803.
[23] L. Du, H.Y. Song, S.J. Liao, Appl. Surf. Sci. 255 (2009) 9365–9370.
[24] S.G. Zhang, L. Xu, H.C. Liu, Y.F. Zhao, Y. Zhang, Q.Y. Wang, Z.X. Yu, Z.M. Liu, Mater. Lett. 63 (2009) 258–259.
[25] X. Gu, C.L. Li, X.H. Liu, J.W. Ren, Y.Q. Wang, Y.L. Guo, Y. Guo, G.Z. Lu, J. Phys. Chem. C 113 (2009) 6472–6479.
[26] H.M. Lin, G.S. Zhu, J.J. Xing, B. Gao, S.L. Qiu, Langmuir 25 (2009) 10159–10164.
[27] T.D. Ewers, A.K. Sra, B.C. Norris, R.E. Cable, C.H. Cheng, D.F. Shantz, R.E. Schaak, Chem. Mater. 17 (2005) 514–520.
[28] H.G. Yang, H.C. Zeng, Angew. Chem. Int. Ed. 43 (2004) 5930–5933.
[29] M.H. Cao, C.W. Hu, Y.H. Wang, Y.H. Guo, C.X. Guo, E.B. Wang, Chem. Commun. 15 (2003) 1884–1885.
[30] J.P. Liu, X.T. Huang, Y.Y. Li, K.M. Sulieman, X. He, F.L. Sun, Cryst. Growth Des. 6 (2006) 1690–1696.
[31] Y. Chang, H.C. Zeng, Cryst. Growth Des. 4 (2004) 397–402.
[32] X.G. Wen, Y.T. Xie, C.L. Choi, K.C. Wan, X.Y. Li, S.H. Yang, Langmuir 21 (2005) 4729–4737.
[33] G.F. Zou, H. Li, D.W. Zhang, K. Xiong, C. Dong, Y.T. Qian, J. Phys. Chem. B 110 (2006) 1632–1637.
[34] H.W. Hou, Y. Xie, Q. Li, Cryst. Growth Des. 5 (2005) 201–205.
[35] S.Y. Gao, S.X. Yang, J. Shu, S.X. Zhang, Z.D. Li, K. Jiang, J. Phys. Chem. C 112 (2008) 19324–19328.
[36] B. Liu, H.C. Zeng, J. Am. Chem. Soc. 126 (2004) 8124–8125.
[37] Q. Peng, Y.J. Dong, Y.D. Li, Angew. Chem. Int. Ed. 42 (2003) 3027–3030.
[38] C.Z. Wu, Y. Xie, L.Y. Lei, S.Q. Hu, C.Z. Yang, Adv. Mater. 18 (2006) 1727–1732.
[39] D. Fan, P.J. Thomas, P. O'Brien, J. Am. Chem. Soc. 130 (2008) 10892–10894.
[40] S.N. Mlondo, P.J. Thomas, P. O'Brien, J. Am. Chem. Soc. 131 (2009) 6072–6073.
[41] Y. Lin, H. Skaff, A. Boker, A.D. Dinsmore, T. Emrick, T.P. Russell, J. Am. Chem. Soc. 125 (2003) 12690–12691.
[42] U.K. Gautam, M. Ghosh, C.N.R. Rao, Langmuir 20 (2004) 10775–10778.
[43] Z. Zhuang, Q. Peng, B. Zhang, Y.J. Li, J. Am. Chem. Soc. 130 (2008) 10482–10483.
[44] H. Xu, F.L. Jia, Z.H. Ai, L.Z. Zhang, Cryst. Growth Des. 7 (2007) 1216–1219.
[45] J. Rudloff, H. Cölfen, Langmuir 20 (2004) 991–996.
[46] H. Wang, J.Z. Xu, J.J. Zhu, H.Y. Chen, J. Cryst. Growth 244 (2002) 88–94.
[47] S.C. Yan, K. Shen, Y. Zhang, Y.P. Zhang, Z.D. Xiao, J. Nanosci. Nanotechnol. 9 (2009) 4886–4891.
[48] S.W. Cao, Y.J. Zhu, J. Phys. Chem. C 112 (2008) 6253–6257.
[49] K. Kočí, L. Obalová, L. Matějová, D. Plachá, Z. Lacnýa, J. Jirkovský, O. Šolcova, Appl. Catal. B: Environ. 89 (2009) 494–502.
[50] M. Hoffmann, S.T. Martin, W. Choi, D.W. Bahnemann, Chem. Rev. 95 (1995) 69–96.
[51] L.Q. Jing, S.D. Li, S. Song, L.P. Xue, H.G. Fu, Sol. Energy Mater. Sol. Cells 92 (2008) 1030–1036.
[52] L. Kronik, Y. Shapira, Surf. Sci. Rep. 37 (1999) 1–5.